Journal of
Advanced Civil and Environmental Engineering
Vol.5, No.1, 2022, pp 11-23
ISSN: 2599-3356
DOI: http://dx.doi.org/10.30659/jacee.5.1.11-23

Experimental Study of RC Hollow Beams with Embedded PVC Pipes

Jen Hua Ling[1*], Joseph Toh Sheng Ngu[1], Yong Tat Lim[1], Wen Kam Leong[1] and How Teck Sia[1]

[1]*Centre for Research of Innovation & Sustainable Development, School of Engineering and Technology, University of Technology Sarawak, 96000 Sibu, Sarawak, Malaysia*

* *Corresponding author: lingjenhua@uts.edu.my*

Abstract: This study investigated the behaviour of reinforced concrete (RC) hollow beams under incremental static loads. Polyvinyl Chloride (PVC) pipes were used to create longitudinal voids in hollow beams. The parameters studied included the size (25 mm, 50 mm and 75 mm diameter) and location (39 mm and 139 mm from beam soffit) of the PVC pipes in the beam. Nine specimens were tested under the four-point load test setup. The loads were progressively increased until the specimens failed. The specimens were analysed based on the failure modes, load-displacement responses and mechanical properties. The hollow beams gave a 2% to 36% lower strength than the solid beams. In terms of the strength per unit concrete, the hollow beams were less efficient than the solid beams. The efficiency ratio of hollow beams ranged from 0.67 to 1.0. For that, none of the proposed hollow beams was recommended.

Keywords: *Hollow section; Longitudinal void; PVC pipe; Reinforced concrete beam*.

1. Introduction

A reinforced concrete (RC) structure comprises elements like beam, slab and column. A beam is a horizontal member in an RC structure. It supports loads of brick walls, adjacent slabs and other service loads. It then transfers the loads to the columns and foundations.

A beam resists loads acting perpendicularly to its longitudinal axis. It bends in this major axis under loads. When overloaded, a beam typically fails due to excessive deflection or extensive cracking. The loads constitute both the external load and the beam's weight. Ideally, the beam's weight should be minimal without compromising the structural performance.

A method to reduce the beam's weight is by creating a longitudinal void along a beam. Researchers embedded Polyvinyl Chloride (PVC) pipes in RC beams to produce hollow beams [1-10]. This is conceptually viable based on the bending theory of a beam. From Fig. 1, the concrete at the tension zone does not contribute to the bending resistance of a beam.

The longitudinal void reduces the cross-sectional area of a beam. This reduces the stiffness and load capacity of the hollow beam [3, 11]. Under flexural load, the deflection of the hollow beam would be higher than a solid beam [3, 11]. The void reduces the shear resistance of the hollow beam. The failure can be brittle if it fails in shear [12], and this should be avoided. These detrimental effects amplify as the hollow ratio increases [11]. The hollow ratio is the area of void relative to the beam cross-sectional area.

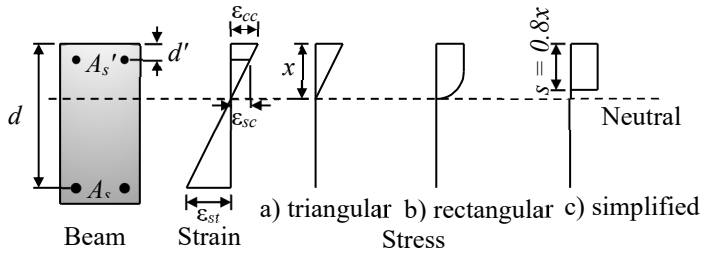

Fig. 1. Stress block diagram of bending theory.

A hollow beam can give a comparable strength as a solid beam if it is properly designed. From Table 1, there were cases when the strength ratios of hollow beams exceeded 1.0. Bhattarai and Bhattarai (2017)[4] and Parthiban and Neelamegam (2017)[9] believed the PVC pipe to have contributed to the beam strength. For good performance of beam, the void should be small [6]. It is more appropriately be placed in the tension zone near the neutral axis [10].

Table 1. Previous studies of hollow beams

Author	Beam size b_b x h_b x l_b (mm x mm x mm)	PVC pipe diameter, d_p (mm)	Position of PVC pipes*[1]	Size-to-depth ratio, d_p/h_b*[2]	Size-to-width ratio, d_p/b_b*[2]	Hollow ratio, $100A_p/A_b$ (%)*[2, 3]	Strength ratio, $P_{u,h}/P_{u,s}$ *[2, 3]
Sherin and Abhirami (2018)[1]	150 x 300 x 1000	25, 32	NA	0.08 - 0.11	0.17 - 0.21	1.09 - 1.79	1.27 - 1.37
Joy and Rajeev (2014)[2]	150 x 230 x 980	40, 50	NA	0.17 - 0.22	0.27 - 0.33	3.64- 5.69	0.96 - 0.97
Murugesan and Narayanan (2016)[6]	150 x 250 x 1700	25, 40, 50	CZ, NA, TZ	0.1 - 0.2	0.17 - 0.33	1.31 - 5.24	0.93 - 1.00
Bhattarai and Bhattarai (2017)[4]	200 x 300 x 2000	50, 60	TZ	0.17 - 0.2	0.25 - 0.3	3.27 - 4.71	1.01 - 1.02
Soji and Anima (2016)[5]	150 x 200 x 1250	38	TZ	0.19	0.25	4.00 – 16.00	1.20 - 1.88
Kuriakose and Paul (2015)[8]	150 x 150 x 700	20, 25	NA	0.13 - 0.17	0.13 - 0.17	1.40 - 2.18	0.98 - 1.02
Parthiban and Neelamegam, (2017)[9]	150 x 200 x 1200	12, 25, 50	TZ	0.18 - 0.25	0.08 - 0.33	0.38 - 6.54	0.60 - 0.93
Varghese and Joy (2016)[10]	200 x 300 x 2000	50	NA, TZ	0.17	0.25	3.27 - 3.27	1.13 - 1.21

**Note:* [1]*CZ – Compression Zone, NA – Neutral Axis, TZ – Tension Zone*
[2]*The values are computed based on the data given by the respective publications*
[3]*A_p – sectional area of PVC pipe, A_b – sectional area of the beam*
[4]*$P_{u,h}$ – Ultimate strength of hollow beam, $P_{u,s}$ – ultimate strength of solid beam*

For some reason, the proposed size of PVC pipes by the researchers barely exceeded 0.25 times the beam height ($d_p \leq 0.25h_b$) or 0.33 times the beam width ($d_p \leq 0.33b_b$) (Table 1). The hollow ratio seldom exceeded 6.5%. This leads to the question of whether a larger pipe size is possible.

With that, an experimental study was carried out on hollow beams. PVC pipes were used to create longitudinal voids in the beams. The effects of the diameter and the position of PVC pipe were investigated.

2. Experimental Program

2.1. Specimen details

Two solid RC beams and nine hollow beams were tested. The details are given in Table 2 and Fig. 2. The beam size was 150 mm x 300 mm x 1650 mm. The clear span was 1500 mm.

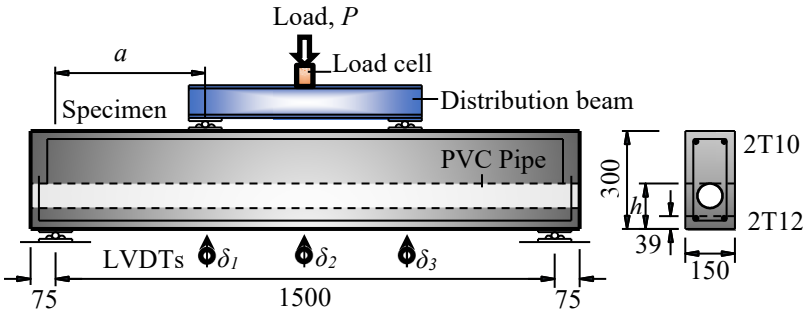

Fig. 2. Test setup.

Table 2. Specimen details

Specimen	PVC pipe		Point load	Shear reinforcement	Remarks
	Position, h (mm)	Diameter, d_p (mm)	Distance from support, a (mm)		
CB1	-	-	600	R8-150	Control, a/d = 2.3
CB2	-	-	500	R8-250	Control, a/d = 1.92
FB1	139	25	600	R8-150	a/d = 2.3
FB2	64	25	600	R8-150	a/d = 2.3
FB3	139	50	600	R8-150	a/d = 2.3
FB4	89	50	600	R8-150	a/d = 2.3
FB5	139	75	600	R8-150	a/d = 2.3
FB6	114	75	600	R8-150	a/d = 2.3
SB7	139	25	500	R8-250	a/d = 1.92
SB8	139	50	500	R8-250	a/d = 1.92
SB9	139	75	500	R8-250	a/d = 1.92

Note: Effective depth of beam, d = 261 mm

Each hollow beam has a PVC pipe embedded throughout the beam span. The pipes were placed at a distance between 39 mm to 139 mm from the beam soffit in the tension region of the beam (Fig. 3). The pipe diameters were 25 mm, 50 mm and 75 mm. The concrete cover was 25 mm.

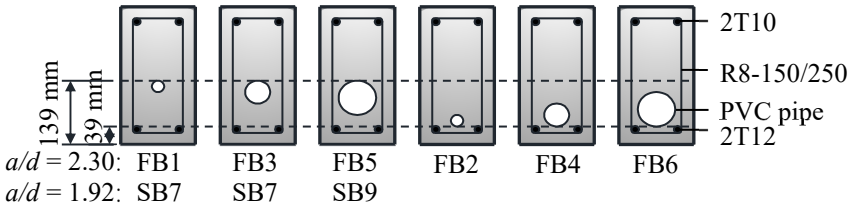

Fig. 3. Position of PVC pipes by specimens.

The reinforcements of the specimens were:

- top reinforcements: 2 units of high yield steel bar (12 mm nominal diameter) with the specified yield strength of 460 N/mm^2
- bottom reinforcements: 2 units of high yield steel bar (10 mm nominal diameter) with the specified yield strength of 460 N/mm^2
- shear links: mild steel bars (8 mm nominal diameter) with the specified yield strength of 250 N/mm^2, which were spaced at 150 mm and 250 mm for specimens FB and SB respectively

The specimens were horizontally cast in plywood moulds using ready-mixed concrete grade 25 (Fig. 4). The maximum aggregate size was 20 mm. The slump was designed in the range of 60 mm to 180 mm. The specimens were cured by preserving water on the beam top surface for at least 7 days. The specimens were placed in an open-air area which was sheltered. The atmosphere temperature was 30 ± 5°C. The specimens were tested after 28 days of casting.

Fig. 4. Fabrication of beam specimens.

2.2. Test Setup

The specimens were placed under a four-point load setup (Fig. 2). A hydraulic cylinder was used to induce load on the specimen. The load was converted into two point-loads by a distribution beam. The point loads sat on the beam at 600 mm and 500 mm distance from the beam supports for specimens FB and SB respectively. The *a/d* ratios of specimens FB and SB were 2.3 and 1.92 respectively. The shear links were more closely spaced in specimens FB (150 mm spacing) than specimens SB (250 mm spacing). The purpose was to enhance the shear resistance of specimens FB to encourage flexural failure at the ultimate state.

Table 3. Instrument specifications

Instruments	Brand, Model	Description	Data accuracy
Hydraulic Cylinder	Enerpac, RR-10018	Push +933kN, Pull -435kN	-
Hydraulic Pump	Enerpac P464	Manual hand pump	-
Displacement transducer	TML, CDP-100	100 mm	0.01 mm
Load Cell	TML, CLJ-300KNB	Capacity 300kN	0.01 kN
Data Logger	TML, TDS-530	30 Channels	-

A load cell was used to measure the load acting on the specimen (Table 3). Three linear variable differential transducers (LVDT) were used to monitor the beam deflection. The LVDTs were placed at the mid-span and below the two point-loads to the beam soffit. All measuring devices were connected to a data logger for data acquisition.

2.3. Test Procedure

Before the test started, the readings of the instruments were set to zero. The beam was preloaded to 10% of the estimated beam capacity for about 5 minutes. The purpose was to consolidate the

test setup. The load was then released for another 5 minutes to observe the reading recovering to zero. This was to check the validity of the measuring devices. This process was repeated twice.

Then, the readings were re-initialised to zero and the test started. The load was increased slowly. At every 5% of the estimated load capacity of the specimen or 0.5 mm of displacement at mid-span (whichever reached first), the load was maintained for at least 1 minute before the readings were taken. The specimen was tested until failure. The test ended as the applied load peaked. This was confirmed by three consecutive drops of the load readings.

The propagation of cracks was visually inspected throughout the test. Markings were made at the ends of the cracks and the corresponding load levels were written on the beam surface. Photos were taken to record the progression of the cracks.

3. Test results

3.1. Material properties

Table 4 shows the concrete strength of the specimens. The results were obtained from the compressive test of concrete cubes. The concrete strength ranged from 24.6 N/mm^2 to 27.8 N/mm^2. It was closed to the designed strength of 25 N/mm^2.

Table 4. Compressive strength of concrete

Specimen	Age (days)	Compressive strength (N/mm^2)	Density (kg/m^3)
CB1	28	26.9	2320
CB2	29	25.9	2329
FB1	30	24.6	2305
FB2	31	25.8	2344
FB3	32	26.3	2349
FB4	35	27.8	2367
FB5	36	26.8	2347
FB6	37	24.9	2300
SB7	38	27.3	2338
SB8	39	26.9	2361
SB9	42	25.6	2335

Note: One unit of 150 mm concrete cube was tested on the day that the specimen was tested to represent its concrete strength

Table 5 presents the tensile strength of steel bars used in the specimens. The yield strengths of the steel bars were higher than the specified yield strengths. The material properties were quite consistent and met the required strength.

Table 5. Properties of steel bars

Bar type	Specified yield strength (N/mm^2)	Tensile strength (N/mm^2)			Average tensile strength (N/mm^2)
		A	B	C	
High yield steel bar	460	532	551	547	543.3
Mild steel bar	250	295	281	278	284.7

3.2. Cracks and failure mode

Fig. 5 shows the crack pattern of the specimens. Three types of cracks were observed, which were flexural crack, flexural-shear crack, and shear crack.

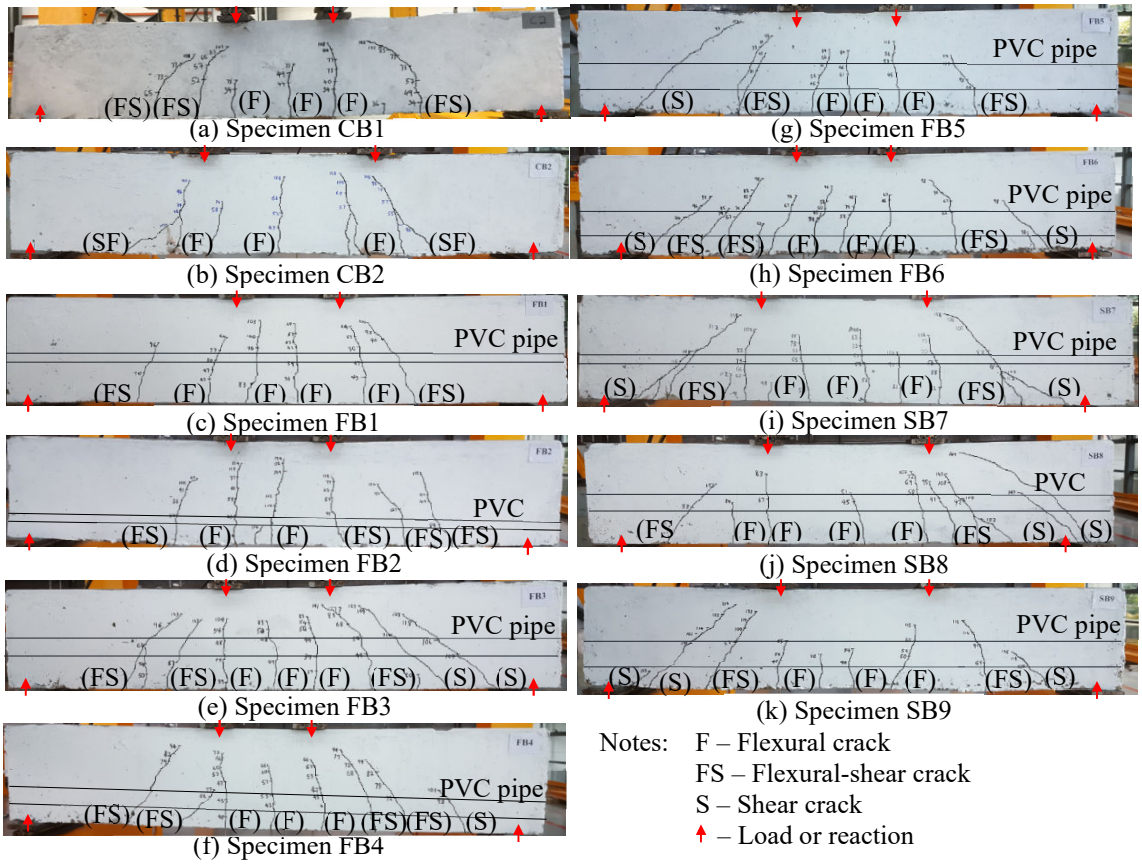

Fig. 5. Crack pattern of specimens.

The flexural crack was first seen at the mid-span. It was noticed around 34 kN to 47 kN load (Table 6). It developed due to excessive beam deflection upon exceeding the concrete strain limit. The crack started from the beam soffit and headed upward. As the load increased, more flexural cracks appeared along the beam. The cracked region expanded from the mid-span to the beam supports. The flexural cracks were typically seen at the region between the two point-loads acting on the beam. The moment-shear ratio (*M/V*) was relatively high in this region.

Table 6. Cracking loads

Specimen	First flexural crack (kN)	First flexural-shear crack (kN)	First shear crack (kN)	Failure mode
CB1	34	34		Flexural
CB2	47	55		Flexural
FB1	36	70		Flexural
FB2	45	84		Flexural
FB3	37	44	104	Diagonal tension
FB4	40	68	98	Diagonal tension
FB5	45	69	93	Shear compression
FB6	38	62	94	Diagonal tension
SB7	45	78	112	Shear compression
SB8	45	83	147	Shear compression
SB9	40	57	100	Shear compression

The flexural-shear cracks were first detected at 34 kN to 84 kN load. These cracks started as vertical cracks due to flexure. They became inclined as they penetrated deeper into the beam. The flexural-shear cracks were found between the point-loads and the beam supports. The *M/V* ratio of this region was moderate.

The shear cracks were the inclined cracks found at the ends of the beam, where the *M/V* ratio was relatively low. The cracks started from the beam support and headed towards the point-loads. The shear crack was seen at high load levels around 93 kN to 147 kN. Not all specimens had a shear crack. The crack was not detected on specimens CB1, CB2, FB1 and FB2. Specimens CB1 and CB2 were solid beams, while specimens FB1 and FB2 had a pipe size of 25 mm. This implied that the longitudinal void indeed reduced the shear resistance of the beam.

Three types of failure mode were observed. This included flexural failure, diagonal tension failure and shear compression failure (Table 7). The failure mode was defined based on the severity of the crack. This included (a) the crack length, (b) the crack width, and (c) the highest load achieved by the cracks. The failure mode of each specimen is listed in Table 6.

Table 7. Type of failure mode

	Flexural failure	**Diagonal tension**	**Shear compression**
Description	• The flexural cracks were dominant. • The flexural-shear crack may or may not be present. • No shear crack was noticed.	• The flexural-shear cracks were dominant. • Shear crack may or may not be present.	• The shear crack was dominant. • The shear crack may or may not reach the top reinforcement in the beam • The top beam may or may not be crushed.
Definition criteria	• The width of the flexural crack was the largest, and/or • The length of the flexural crack was the longest, and/or • The recorded load for the flexural crack was the highest	• The width of the flexural-shear crack was the largest, and/or • The length of the flexural-shear crack was the longest or at least comparable to the shear crack, and/or • The recorded load for the flexural-shear crack was the highest	• The width of the shear crack was the largest, and/or • The length of the shear crack was the longest, and/or • The recorded load for the shear crack was the highest

Specimens with small pipe diameters ($d_p \leq 25$ mm) experienced flexural failure (Table 6). This included specimens CB1, CB2, FB1 and FB2. Specimens with large pipe diameters ($d_p \geq 50$ mm) failed either by diagonal tensile failure or shear compression failure. This was subjected to (a) the *a/d* ratio used in the test setup, and (b) the amount of shear link provided.

Specimens FB3, FB4 and FB6 had a larger *a/d* ratio of 2.3. The shear links were more closely spaced. These specimens endured diagonal tension failure. Specimens SB7, SB8 and SB9 were tested with a smaller *a/d* ratio of 1.92. Fewer shear links were provided. These specimens failed by shear compression failure. Low *a/d* ratio had the point load placed closer to the support. This increased the shear stress in the beam. As lightly reinforced in shear, the hollow beams were susceptible to shear failure.

3.3. Load response

Fig. 6 shows the load response of the specimens. During the test, the applied loads and the mid-span displacements were recorded. The results were plotted into the load-displacement curves. In general, the hollow beams showed a similar behaviour as an RC beam; (a) the beams experienced bending deformation under loads, (b) the deflections increased as the loads increased, (c) the rate of increment progressively changed throughout the test.

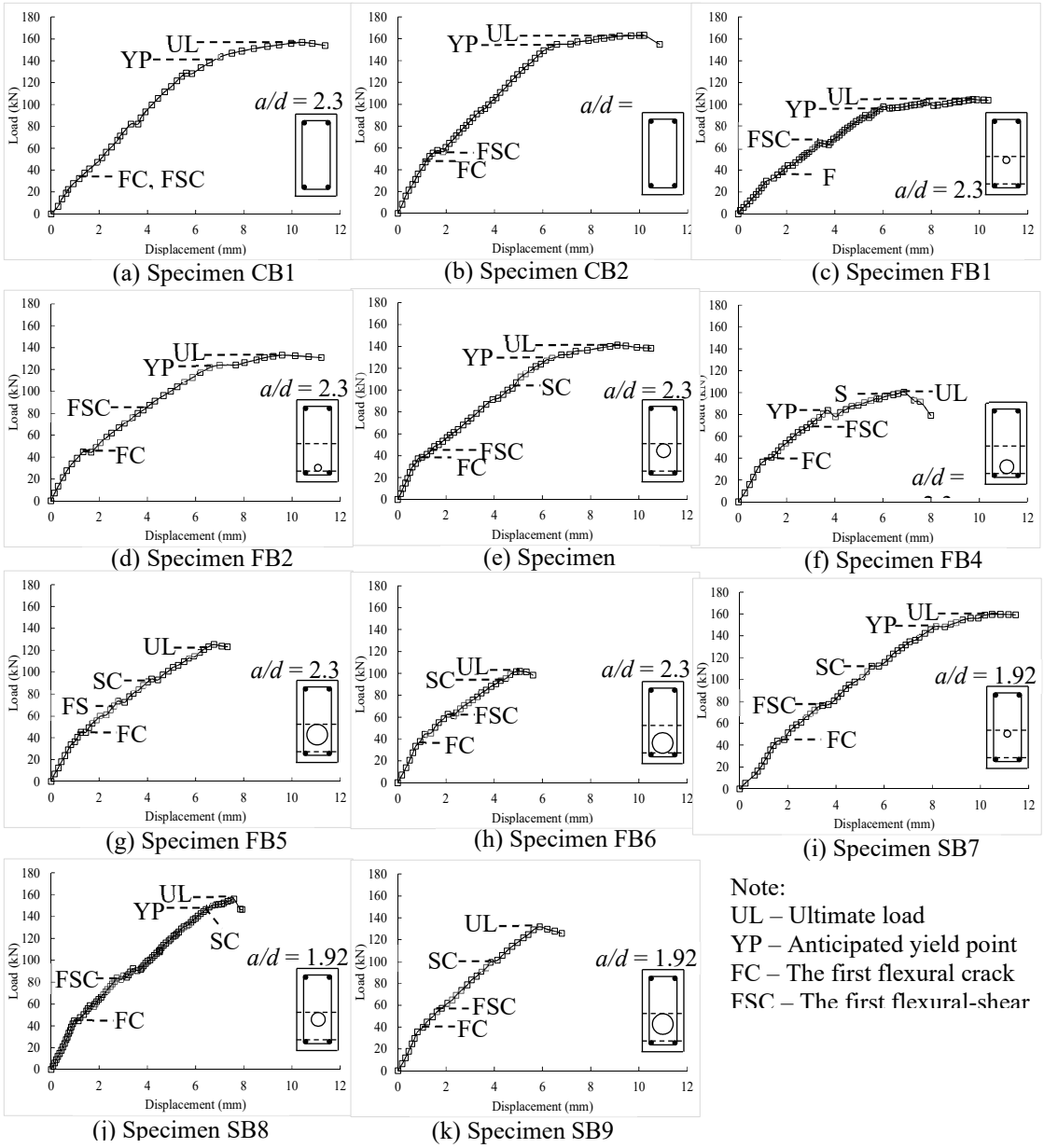

Fig. 6. Load-displacement response.

The slope of the load-displacement curve represented the stiffness of the specimen. A steep slope indicates a high stiffness and vice versa. The hollow beams started with high stiffness. Before the propagation of cracks, the stiffness was the highest and the deflection progressed slowly.

The stiffness reduced slightly as the first crack propagated. The flexural crack developed first. This was followed by the flexural-shear crack and the shear crack. These cracks gradually deteriorated the stiffness and caused the deflection to develop at a faster rate.

Reaching the ultimate state, specimens FB1, FB2, FB3, FB4, SB7 and SB8 demonstrated symptoms of yielding. The stiffness dropped drastically and the deflection developed rapidly. This was likely due to the yielding of the tension steel bars. However, as strain gauges were not installed on the tension steel bars, it was unsure if the steel bars did yield. Nevertheless, the specimens gave a ductile behaviour.

On the other hand, specimens FB5, FB6 and SB9 did not show clear symptoms of yielding. These specimens were relatively brittle. They suddenly failed without experiencing a drastic change of stiffness. The large void (75 mm diameter) seemed to affect the shear capacity of these hollow beams. Thus, severe shear cracks and flexural-shear cracks were detected.

At the ultimate state, the hollow beams experienced critical damages. Extensive cracking affected the bond between the concrete and the tension steel bars. This prevented the beams to carry higher loads. The hollow beams reached their load capacities as the load-displacement curves peaked. Beyond that, the beams were considered failed.

3.4. Mechanical properties

Table 8 presents various properties of the specimens. This includes secant stiffness, yield point, ultimate load and ultimate displacement. These properties were computed from the load-displacement curves using the method proposed by Park (1988) [13] and Noushini et al. (2014) [14] (Fig. 7).

Table 8. Properties of specimens

Specimen	Secant stiffness, S (kN/mm)	Yield strength, P_y (kN)	Yield Displacement, δ_y (mm)	Ultimate load, P_u (kN)	At mid-span displacement, δ_u (mm)
CB1	23.3	140	6.73	156.8	10.42
CB2	25.8	152.2	6.32	163.1	10.2
FB1	17.3	97.7	6.06	104.8	9.73
FB2	20.2	122.4	6.59	133.1	9.59
FB3	21.7	130.8	6.51	141.2	9.11
FB4	23.4	82.5	4.29	100.4	6.87
FB5	21.0	-	-	125.2	6.76
FB6	24.2	-	-	101.8	5.07
SB7	19.2	148.4	8.31	159.6	10.48
SB8	24.1	147.1	6.47	156.0	7.59
SB9	25.9	-	-	131.7	5.88

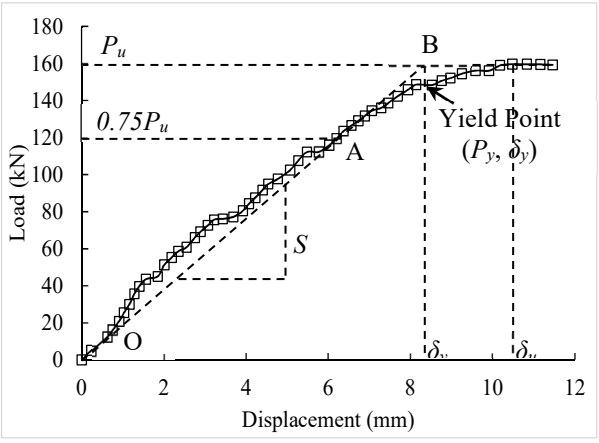

Fig. 7. Beam properties of a typical load-displacement response.

The peak of the load-displacement curve resembled the ultimate load, P_u. The displacement corresponding to P_u was the ultimate displacement, δ_u. Two horizontal lines were then constructed at P_u and 0.75 times P_u. A straight line was drawn connecting the origin (denoted as "O" in Fig. 7) and the intersection point between the $0.75P_u$ horizontal line and the load-displacement curve (denoted as "A" in Fig. 7).

The gradient of this straight line was considered the secant stiffness of the specimen, *S*. This secant stiffness line was subsequently extended to intercept with the P_u horizontal line (point B in Fig. 7). The yield point was anticipated to be a point on the load-displacement curve below that interception. This yield point was then checked against the yielding symptoms. If no noticeable reduction of stiffness was detected, the specimen was considered without a yield point.

4. Structural performance

Table 9 recomputes the results from Table 6 and Table 7. The load, P_{ic}, and moment, M_{ic}, when the first crack was detected were identified. The shear load, V_u, and bending moment, M_u, when the specimens failed were determined. These values were computed based on Fig. 8 using Equation 1 and Equation 2.

$$V = \frac{P}{2} \tag{1}$$

$$M = \frac{Pa}{2} \tag{2}$$

where V = shear load (kN)
M = bening moment (kNm)
P = load applied on the specimens (kN)
a = distance between the beam support and the point load (m)

Table 9. Computed results

	First crack load, P_{ic} (kN)	**First crack moment, M_{ic} (kNm)**	**Shear load, V_u (kN)**	**Moment, M_u (kNm)**	**Crack-to-ult. strength ratio, P_{ic}/P_u**	**Yield-to-ult. strength ratio, P_y/P_u***	**Ductility ratio, $\Delta = \delta_u/\delta_y$***
Ref.	Table 6	Eq. 2	Eq. 1	Eq. 2	Table 8	Table 8	Table 8
CB1	34	10.2	78.4	47.0	0.22	0.89	1.55
CB2	47	11.8	81.6	40.8	0.29	0.93	1.61
FB1	36	10.8	52.4	31.4	0.34	0.93	1.61
FB2	45	13.5	66.6	39.9	0.34	0.92	1.46
FB3	37	11.1	70.6	42.4	0.26	0.93	1.40
FB4	40	12.0	50.2	30.1	0.40	0.82	1.60
FB5	45	13.5	62.6	37.6	0.36	1.00	1.00
FB6	38	11.4	50.9	30.5	0.37	1.00	1.00
SB7	45	11.3	79.8	39.9	0.28	0.93	1.26
SB8	45	11.3	78.0	39.0	0.29	0.94	1.17
SB9	40	10.0	65.9	32.9	0.30	1.00	1.00

**Note: In the absence of yield point, P_y/P_u and δ_u/δ_y ratios were taken as 1.0*

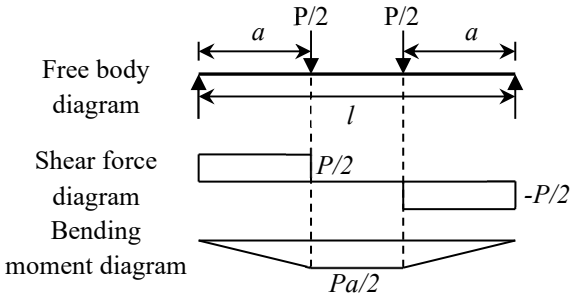

Fig. 8. Shear force and bending moment acting on beam.

In hollow beams, the first crack developed around 1/3 of the ultimate capacities. The P_{ic}/P_u ratios of the hollow beams ranged from 0.26 to 0.40 (Table 9). The first crack developed about the same time as the solid beam.

The hollow beams had a limited strength upside after yield points before failure. Most of them had P_y/P_u ratios close to 1.0. The strength upside of the hollow beams was typically lower than the solid beams. This shall indirectly affect the ductility response of the hollow beam.

The ductility ratios of the hollow beams were generally lower than the solid beams. The larger the size of the longitudinal void, the lower the ductility. This can be seen from specimens FB5, FB6 and SB9. These specimens had the largest pipe size (i.e. 75 mm diameter) but the ductility ratios were the smallest (Δ = 1.0). The specimens failed without clear symptoms of yielding. This was in line with the finding by Inoue and Egawa (1996) [12] when shear load was more dominant.

The hollow beams had a lower strength than the solid beams. The strength ratios, R_s, ranged between 0.64 and 0.98 (Table 10). This was mainly due to the smaller cross-sectional area and second moment of area of the hollow beams. The reduced cross-sectional area affected the shear strength, while the small second moment of area reduced the flexural strength of hollow beams.

Table 10. Efficiency of hollow beams

	Size-to-height ratio, = d_p/h_b	**Size-to-height ratio, = d_p/b_b**	**Hollow ratio, = A_p/A_b**	**Effective area ratio, $A_{eff} = (A_b - A_p)/A_b$**	**Strength ratio, $R_s = P_{u,h}/P_{u,s}$**	**Efficiency ratio, $R_{eff} = R_{us}/A_{eff}$**
FB1	0.083	0.167	0.011	0.99	0.67	0.68
FB2	0.083	0.167	0.011	0.99	0.85	0.86
FB3	0.167	0.333	0.044	0.96	0.90	0.94
FB4	0.167	0.333	0.044	0.96	0.64	0.67
FB5	0.250	0.500	0.098	0.90	0.80	0.89
FB6	0.250	0.500	0.098	0.90	0.65	0.72
SB7	0.083	0.167	0.011	0.99	0.98	0.99
SB8	0.167	0.333	0.044	0.96	0.96	1.00
SB9	0.250	0.500	0.098	0.90	0.81	0.90

Notes: d_p = diameter of PVC pipe (mm), h_b = height of beam (mm), b_b = width of beam (mm), A_p = area of longitudinal void (mm^2), A_b = area of beam (mm^2), $P_{u,h}$ = ultimate strength of hollow beam, $P_{u,s}$ = ultimate strength of solid beam.

The hollow beam was less efficient than the solid beam. This can be seen from the efficiency ratio, R_{eff}, which ranged from 0.67 to 1.0 (Table 10). When R_{eff} was less than 1.0, the hollow beam lost more strength than the cross-sectional area by percentage. As a result, the load capacity per unit of concrete of the hollow beams was lower than the solid beams. On this basis, longitudinal void in an RC beam is not recommended. This is unless (a) there are solid reasons for the existence of PVC pipe in the beam, and/or (b) there are feasible mechanisms to strengthen the hollow beam.

5. Limitations of study

In this study, only one specimen was tested for each design. The data was limited. Based on the current set of data, it is hard to tell the best location and the optimum size of the longitudinal void in a hollow beam.

It seems that placing PVC pipe close to the beam soffit led to a lower strength ratio. This can be observed from specimens FB3, FB4, FB5 and FB6 (Table 10). However, specimens FB1 and FB2

implied the opposite. Based on the study by Varghese and Joy (2016) [10], the PVC pipe should be placed just below the neutral axis.

The effect of pipe size on the beam strength was not clearly seen. Specimens with small pipes seemed to have higher strength ratios than those with larger pipes. This can be seen from specimens FB2 and SB7 as their strength ratios were the highest within their specimen groups. However, this was not necessarily true among specimens FB1, FB3 and FB5. Specimen FB3 (50 mm pipe diameter) was stronger than specimens FB1 and FB5. Nevertheless, the hollow beam with a larger pipe size was expected to give a lower strength [11].

Solely based on the bending theory in Fig. 1, the presence of the longitudinal void should not affect the ultimate strength of a hollow beam. As long as the pipe is located below the neutral axis, it is regardless of the size and location of the pipe. According to Bhattarai and Bhattarai (2017)[4] and Parthiban and Neelamegam (2017)[9], the bending resistance of PVC pipe offers additional strength to the hollow beam. The surrounding concrete helps to keep the PVC pipe in shape during bending. It is possible for PVC pipe to offer bending strength to the beam.

Based on the results in this study, the longitudinal void indeed affected the beam strength. There could be other factors, which are unknown at this moment, leading to this outcome. As the bending strength of PVC pipe was not quantified, it is unsure whether the PVC pipe did contribute to the beam strength.

To overcome the abovementioned limitations, further study is required. For better consistency of the results, three identical specimens may be required for each design configuration. One may also model the hollow beams using the finite element method to simulate the load responses, especially in terms of the internal stresses.

6. Conclusion

The behaviour of nine RC hollow beams was investigated by experimental studies. The longitudinal void affected the performance of the hollow beams. The strength, ductility and efficiency of the hollow beam were slightly lower than the solid RC beam. Due to limited data available, the best location and the optimum size of the longitudinal void in a hollow beam were unable to be defined.

Acknowledgements

This work was supported by the Research Grants of University College of Technology Sarawak, UCTS/RESEARCH/2/2018/02.

References

[1] Sherin, K. and Abhirami, S. (2018). Analytical Study on Geopolymer Concrete Beam with Hollow Space Below Neutral Axis, *International Journal of Advance Engineering and Research Development*, *5*(5), 332-342.

[2] Joy, J., Rajeev, R. (2014). Effect of Reinforced Concrete Beam with Hollow Neutral Axis *International Journal for Scientific Research & Development, 2*(10), 341-348.

[3] Ragavi, L. (2017). Behaviour of Reinforced Concrete Hollow Beams under Monotonic Loading, *World Journal of Technology, Engineering and Research, 2*(1), 127-136.

[4] Bhattarai, B.P. and Bhattarai, N. (2017). Experimental Study on Flexural Behavior of Reinforced Solid and Hollow Concrete Beams, *International Journal of Engineering Research and Advanced Technology, 3*(11)*,* 1-8.

[5] Soji, S. and Anima, P. (2016). Experimental and Analytical Investigation on Partial Replacement of Concrete in the Tension Zone, *International Journal of Engineering Research and General Science, 4*(4)*,* 23-32.
[6] Murugesan, A. and Narayanan, A. (2016). Influence of a Longitudinal Circular Hole on Flexural Strength of Reinforced Concrete Beams, *Practice Periodical on Structural Design and Construction, 22*(2), 04016021, 1-10.
[7] Dhinesh, N.P. and Satheesh, V.S. (2017). Flexural Behaviour of Hollow Square Beam, *International Journal of Scientific Engineering and Applied Science*, *3*(3)*,* 236-242.
[8] Kuriakose, A.M. and Paul, M.M. (2015) Behaviour of Beams with Low Grade Concrete or Hollow Neutral Axis Zone, *International Journal of Civil Engineering and Technology*, *6*(10), 185-190.
[9] Parthiban, N. and Neelamegam, M. (2017). Flexural Behavior of Reinforced Concrete Beam With Hollow Core in Shear Section, *International Research Journal of Engineering and Technology*, *4*(4), 2263-2274.
[10] Varghese, N., Joy, A. (2016). Flexural Behaviour of Reinforced Concrete Beam with Hollow Core at Various Depth, *International Journal of Science and Research*, *5*(5), 741-756.
[11] Alshimmeri, A.J.H. and Al-Maliki, H.N.G. (2014). Structural Behavior of Reinforced Concrete Hollow Beams under Partial Uniformly Distributed Load, *Journal of Engineering, 20*(7), 130-145.
[12] Inoue, S. and Egawa, N. (1996). Flexural and Shear Behaviour of Reinforced Concrete Hollow Beams under Reversed Cyclic Loads, *Eleventh World Conference on Earthquake Engineering*.
[13] Park, R. (1988). Ductility Evaluation from Laboratory and Analytical Testing, *The 9th world conference on earthquake engineering*, Tokyo-Kyoto, Japan, 605-616.
[14] Noushini, A., Samali, B. and Vessalas, K. (2014). Performance of Concrete Beam Elements Reinforced with Polyvinyl Alcohol (PVA) Micro Fibres, *Concrete in Australia, 40*(1), 22-27.